

A PBN-RL-XAI Framework for Discovering a “Hit-and-Run” Therapeutic Strategy in Melanoma

Zhonglin Liu

Department of Mathematics
The University of Hong Kong
Hong Kong SAR, China
u3597461@connect.hku.hk

Abstract—Innate resistance to anti-PD-1 immunotherapy remains a major clinical challenge in metastatic melanoma, with the underlying molecular networks being poorly understood. To address this, we constructed a dynamic Probabilistic Boolean Network model using transcriptomic data from patient tumor biopsies to elucidate the regulatory logic governing therapy response. We then employed a reinforcement learning agent to systematically discover optimal, multi-step therapeutic interventions and used explainable artificial intelligence to mechanistically interpret the agent’s control policy. The analysis revealed that a precisely timed, 4-step temporary inhibition of the lysyl oxidase like 2 protein (LOXL2) was the most effective strategy. Our explainable analysis showed that this “hit-and-run” intervention is sufficient to erase the molecular signature driving resistance, allowing the network to self-correct without requiring sustained intervention. This study presents a novel, time-dependent therapeutic hypothesis for overcoming immunotherapy resistance and provides a powerful computational framework for identifying non-obvious intervention protocols in complex biological systems.

Index Terms—Probabilistic Boolean Networks, Melanoma, Immunotherapy Resistance, Systems Biology, Explainable AI.

I. INTRODUCTION

Immune checkpoint blockade targeting the programmed death-1 (PD-1) pathway has revolutionized treatment for metastatic melanoma, yet innate resistance affects 60-70% of patients [1]. Unlike acquired resistance that develops during treatment, innate resistance manifests as immediate therapeutic failure, suggesting pre-existing molecular networks that render tumors refractory to immune activation from the outset. The mechanistic basis for this variation in response patterns remains poorly explained, representing a critical unmet clinical need.

Recent transcriptomic analyses have identified gene expression signatures associated with resistance, most notably the Innate anti-PD-1 Resistance (IPRES) signature, which encompasses genes involved in mesenchymal transition, extracellular matrix remodeling, angiogenesis, and wound healing [1]. However, the regulatory logic governing how these genes interact dynamically to establish and maintain resistant phenotypes remains largely opaque. Traditional reductionist

approaches focusing on individual biomarkers have failed to capture the systems-level properties that govern therapeutic response, largely due to the inherent complexity of the underlying gene regulatory networks (GRNs) [2].

The challenge of understanding resistance networks is compounded by their dynamic and stochastic nature. Gene regulatory networks exhibit complex emergent behaviors, including multistability, where identical genetic backgrounds can give rise to distinct cellular phenotypes depending on the network’s dynamical state. These systems can become trapped in stable attractor states corresponding to different cellular phenotypes, such as therapy resistance [3]. Identifying effective therapeutic interventions requires understanding not only the static architecture of these networks but also their dynamic properties and control mechanisms.

Current therapeutic discovery approaches face fundamental limitations when applied to complex resistance networks. The vast combinatorial space of possible multi-gene interventions makes exhaustive experimental screening prohibitive. Moreover, optimal intervention strategies may involve precisely timed, transient perturbations rather than sustained pathway inhibition [4], and the stochastic nature of biological networks necessitates probabilistic control strategies.

Probabilistic Boolean Networks (PBNs) offer a powerful framework for modeling gene regulatory systems, combining computational tractability with biological realism through stochastic dynamics [5]. PBNs have successfully modeled various biological phenomena, including cell cycle regulation and cancer progression [6]. Concurrently, advances in reinforcement learning (RL) have opened new avenues for discovering optimal control strategies in complex dynamic systems [7]. Unlike traditional optimization approaches requiring explicit system knowledge, RL agents learn optimal policies through environment interaction, showing promise in biological control applications [8].

Here, we present a novel computational framework integrating PBN modeling with reinforcement learning to systematically discover optimal therapeutic interventions for overcoming innate anti-PD-1 resistance in melanoma. We constructed dynamic PBN models from patient transcriptomic data to capture the regulatory logic governing therapy response, then employed RL agents to identify multi-step intervention

strategies. Using explainable artificial intelligence, we mechanistically interpreted the learned control policies to understand their biological basis.

Our analysis reveals that innate resistance corresponds to a fundamental system-level transition from a plastic, multi-stable network state to a rigid, canalized landscape dominated by a JUN/LOXL2 regulatory axis. Most significantly, our RL approach discovered a non-obvious “hit-and-run” therapeutic strategy: a precisely timed, 4-step temporary inhibition of LOXL2 achieving 93.45% success rate in silico. Explainable AI analysis demonstrated that this transient intervention effectively erases the molecular vulnerability signature driving resistance, allowing the network’s intrinsic dynamics to complete the therapeutic transition without sustained intervention.

This work provides the first application of integrated PBN-RL-explainable AI(XAI) methodology to cancer immunotherapy resistance, offering a generalizable framework for discovering time-dependent therapeutic strategies in complex biological systems. Our work is organized as follows. Section II details our methodology, from data acquisition and network inference to the reinforcement learning and XAI frameworks. Section III presents the results, including the characterization of the resistant network and the discovery and validation of optimal control strategies. Finally, Section IV discusses the implications of our findings and concludes the paper.

II. METHODS

A. Data Acquisition and Binarization

We utilized the landmark RNA-sequencing dataset from Hugo et al. [1], publicly available from the Gene Expression Omnibus (accession: GSE78220). Pre-treatment tumor biopsies were stratified into “Responders” (n=15), defined as patients with a Complete or Partial Response, and “Non-Responders” (n=12), defined as patients with Progressive Disease. One on-treatment sample was excluded to ensure the analysis focused exclusively on the innate resistance state. For biological interpretation, gene identifiers in the raw data were mapped to official HUGO Gene Symbols.

To prepare the data for Boolean modeling, the continuous gene expression values were converted into discrete binary states of 0 (OFF/low activity) or 1 (ON/high activity). The analysis began with the raw count matrix, which was first filtered to include only the core genes. To stabilize the variance across the range of mean expression values, a Variance Stabilizing Transformation (VST) [9] was applied to the filtered count data using the DESeq2 R package [10]. The resulting normalized matrix was then separated into two sub-matrices, one for each cohort.

For each gene within each cohort’s VST-normalized matrix, we employed a Gaussian Mixture Model (GMM) [11] to determine a data-driven binarization threshold. This model-based approach was chosen over simpler methods like a median split because it provides a more principled cutoff. GMM assumes that the observed expression values are generated from two underlying distributions representing ‘low’ and ‘high’ activity states, and it mathematically identifies the threshold that best

separates these putative states rather than imposing an arbitrary split.

Mathematically, the probability density of an expression value x for a given gene is modeled as a weighted sum of two Gaussian components:

$$p(x) = \pi_1 \mathcal{N}(x|\mu_{\text{low}}, \sigma^2) + \pi_2 \mathcal{N}(x|\mu_{\text{high}}, \sigma^2) \quad (1)$$

where π_1 and π_2 are the mixing coefficients that sum to 1, $\mathcal{N}(x|\mu, \sigma^2)$ is the Gaussian probability density function, and $(\mu_{\text{low}}, \mu_{\text{high}}, \sigma^2)$ are the means and common variance of the two components, respectively. These parameters were fitted to the expression data for each gene using the mclust R package. The binarization threshold T was then defined as the midpoint between the means of the two fitted components, $T = (\mu_{\text{low}} + \mu_{\text{high}})/2$. Samples with an expression value greater than this threshold were assigned a state of 1, while those with values less than or equal to the threshold were assigned a state of 0. This process yielded two final binarized matrices that served as the direct inputs for the subsequent network inference.

B. Introduction of PBN

To capture the complex and stochastic nature of gene regulatory networks (GRNs), we employ the Probabilistic Boolean Network (PBN) framework [5]. A PBN is a discrete-time dynamical system that models a set of genes as binary variables, where the state of each gene (ON=1, OFF=0) is updated at each time step according to a set of probabilistic rules.

A PBN is formally defined by a set of n genes, $G = \{g_1, g_2, \dots, g_n\}$. The state of the network at time t is given by a binary vector $\mathbf{x}(t) = (x_1(t), x_2(t), \dots, x_n(t))$, where $x_i(t) \in \{0, 1\}$ is the state of gene g_i .

For each gene g_i , there exists a set of k_i possible Boolean predictor functions, $F_i = \{f_1^{(i)}, f_2^{(i)}, \dots, f_{k_i}^{(i)}\}$. Each function $f_j^{(i)} : \{0, 1\}^n \rightarrow \{0, 1\}$ determines the next state of gene g_i based on the current state of all genes in the network. At each time step t , a single function $f_j^{(i)}$ is selected from the set F_i with a corresponding probability $c_j^{(i)}$, where:

$$P(f = f_j^{(i)}) = c_j^{(i)} \quad \text{and} \quad \sum_{j=1}^{k_i} c_j^{(i)} = 1 \quad (2)$$

The state of gene g_i at the next time step, $t + 1$, is then determined by the selected function: $x_i(t + 1) = f_j^{(i)}(\mathbf{x}(t))$. The selection of a predictor function for each gene is an independent event, defining the transition probabilities between the 2^n possible states of the network.

The long-term behavior of a PBN is characterized by its attractors. An attractor is a set of states from which the network cannot escape once entered. Mathematically, a non-empty set of states A is an attractor if it is a minimal set for which the probability of transitioning from any state $\mathbf{x} \in A$ to any state $\mathbf{y} \notin A$ is zero. These attractors can be a single steady state (a point attractor) or a set of states visited cyclically (a cycle attractor). In the context of systems biology, attractors represent the stable, long-term phenotypes of the cell, such

as proliferation, apoptosis, or in our case, a therapy-resistant state [12].

To quantify the regulatory impact of one gene on another within the network, we utilize the influence of gene g_j on gene g_i . This influence is based on the concept of the sensitivity of the Boolean predictor functions. The influence of g_j on g_i with respect to a specific function $f_k^{(i)}$ is the probability that flipping the state of g_j will flip the output of $f_k^{(i)}$. The total influence, $I(g_j \rightarrow g_i)$, is the expected sensitivity, averaged over all possible predictor functions for gene g_i :

$$I(g_j \rightarrow g_i) = \sum_{k=1}^{k_i} c_k^{(i)} \cdot S(f_k^{(i)}, g_j) \quad (3)$$

where $S(f_k^{(i)}, g_j)$ is the sensitivity of function $f_k^{(i)}$ to gene g_j . The influence matrix, composed of these values, provides a quantitative map of the network's regulatory structure.

C. PKN-constrained PBN construction

The inference of Probabilistic Boolean Networks (PBNs) from data is an NP-hard problem, where the search space for regulatory logic grows double-exponentially with the number of inputs to a given gene, making the analysis of large-scale networks computationally infeasible. Therefore, a critical preliminary step is to constrain the problem space by identifying a core set of the most biologically relevant and dynamically active genes. To this end, we implemented a multi-stage procedure to construct a high-confidence, context-specific Prior Knowledge Network (PKN) that serves as the basis for our tractable PBN model.

1) *Initial network foundation*: The process began with a broad, literature-based network that was systematically refined into a compact, data-driven core network. The initial network foundation was based on the Kyoto Encyclopedia of Genes and Genomes (KEGG) pathway hsa05235, "PD-L1 expression and PD-1 checkpoint pathway in cancer," chosen for its direct relevance to the therapeutic mechanism under investigation. The pathway data was obtained in KGML format, and all constituent gene-gene interactions were parsed and mapped to their corresponding HUGO Gene Symbols.

2) *Hybrid gene selection strategy*: To distill this foundational network into a focused set of key regulators, we devised a hybrid selection strategy combining mandatory inclusion of expert-defined markers with a data-driven ranking of all other genes. This approach guaranteed the inclusion of five core genes from the Innate anti-PD-1 Resistance (IPRES) signature: AXL, ROR2, WNT5A, LOXL2, and TAGLN. The remaining positions in the core gene list were filled by ranking genes based on a composite score derived from two metrics.

The first metric, a Differential Expression Score (S_{DE}), was calculated as the negative base-10 logarithm of the Benjamini-Hochberg adjusted p-value ($-\log_{10}(p_{adj})$) [13] from a differential expression analysis [14] between the responder and non-responder cohorts. The second metric, a Network Influence Score (S_{Net}), was calculated from a data-driven gene

regulatory network inferred by dynGENIE3 [15], capturing a gene's overall importance as both a regulator and a target.

For the final PKN assembly, both the S_{DE} and S_{Net} scores were min-max normalized to a [0, 1] scale. The final data-driven score for each gene was calculated using the equally weighted formula:

$$S_{final} = (0.5 \cdot S_{DE, norm}) + (0.5 \cdot S_{Net, norm}) \quad (4)$$

The final core gene list was created by taking the union of the five mandatory IPRES genes and the top 12 genes from this data-driven ranking. The final PKN was then constructed by extracting the subnetwork from the dynGENIE3-inferred weight matrix corresponding only to the interactions among these selected core genes.

3) *PBN inference methodology*: With the binarized data for the Responder and Non-Responder cohorts, we inferred two distinct PBN models. The inference strategy was designed to identify the most informative regulatory logic for each gene while mitigating the risk of overfitting the model to noise in the data.

The process began by constraining the search space for potential regulators for each target gene. This is a critical step for computational tractability, as testing all possible gene combinations is infeasible. We used the global gene-gene interaction rankings previously generated by dynGENIE3 as a data-driven prior. For each target gene, we selected its top-ranked regulators from this list to form a candidate pool, limiting the pool size to a maximum of 10 genes to balance biological comprehensiveness with computational efficiency.

A key challenge in network inference is selecting the correct number of input regulators, k , for each gene's predictive function. A model that is too simple (small k) may underfit and miss critical interactions, while one that is too complex (large k) may overfit by modeling noise. To navigate this trade-off, we implemented a data-driven selection criterion based on maximizing the Mutual Information (MI). For each target gene, our algorithm iteratively tested regulator sets of increasing size (up to a maximum of $k_{max} = 4$). At each value of k , the algorithm identified the single best-predicting Boolean function from all 2^{2^k} possibilities and calculated its MI score with the target gene's observed data. The optimal number of regulators, k^* , was chosen as the value of k that yielded the function with the maximum MI score.

With an optimal regulator set of size k^* identified for a given target gene, its probabilistic Boolean update rule was defined. To account for biological stochasticity and measurement noise, we constructed a probabilistic ensemble of the most likely functions rather than selecting only the single best predictor. All $2^{2^{k^*}}$ possible Boolean functions were scored using their normalized Mutual Information (MI) [16] value, and the top $N = 4$ functions were selected to form the function set $\{f_1, f_2, \dots, f_N\}$ for that gene. The probability $P(f_i)$ of each function was then assigned proportionally to its MI score, as follows:

$$P(f_i) = \frac{MI(f_i)}{\sum_{j=1}^N MI(f_j)} \quad (5)$$

where $MI(f_i)$ is the Mutual Information score of function f_i . An alternative ranking approach using the Coefficient of Determination (CoD) [17] was considered; however, it was found to be impractical as it produced negative values for some functions in our dataset, making MI a more robust metric for this application.

This entire procedure was performed independently for every gene in both the responder and non-responder datasets, yielding the two final, context-specific PBN models used for all subsequent analysis.

D. Reinforcement Learning for Optimal Dynamic Control

To discover an optimal intervention strategy in a complex biological network, we framed the control of the resistant-state PBN as a reinforcement learning (RL) problem. The state space of the PBN is vast (2^n states), rendering methods based on exhaustive search computationally intractable. Furthermore, the inherent stochasticity of the network means a fixed sequence of interventions does not guarantee a specific outcome. RL is well-suited for finding optimal policies in such large, stochastic environments. To formulate the control problem, we utilized the *gym-PBN* software package, a toolkit designed for the analysis and RL control of Probabilistic Boolean Networks within the Gymnasium framework [18].

We formally model the control problem as a *Markov Decision Process* (MDP) [19]. The *state space*, \mathcal{S} , comprises the 2^n possible binary states, \mathbf{x} , of the PBN. The *action space*, \mathcal{A} , is a set of discrete actions including “Do Nothing” and flipping the state of any single gene. The *transition probabilities*, $P(\mathbf{x}_{t+1}|\mathbf{x}_t, a_t)$, are implicitly defined by the PBN’s update rules under a given action. To model the clinical time constraint, we set the maximum steps to be 15. Finally, the *reward function*, R , was designed to guide the agent: a large positive reward (+100) is given for reaching the target sensitive state, and a penalty (−5) for ending an episode in a known resistant attractor. The action cost is set to 0 so that the agent is not prevented from imposing actions during the 15 steps horizon. The agent’s goal is to learn a *policy*, $\pi(a_t|\mathbf{x}_t)$, that maximizes the expected cumulative reward.

We chose Proximal Policy Optimization (PPO) as our learning algorithm due to its state-of-the-art performance and stability [20]. PPO is a policy gradient method that constrains policy updates by clipping the probability ratio $r_t(\theta) = \frac{\pi_\theta(a_t|\mathbf{x}_t)}{\pi_{\theta_{old}}(a_t|\mathbf{x}_t)}$ between new and old policies, preventing large, destabilizing updates. We utilized the PPO agent from the *Stable-baselines3* library [21] with a multi-layer perceptron policy and trained for 500,000 total timesteps.

E. Sequential Intervention and Explainable AI Analysis

1) *Optimal “Hit-and-Run” Strategy Identification*: To identify a more clinically translatable strategy, we also sought to find an optimal transient intervention. We designed a sequential experiment to test a “hit-and-run” therapeutic model, where the rationale is that a brief, initial perturbation may be sufficient to destabilize the resistant state, allowing the network’s own dynamics to resolve towards a sensitive phenotype

without sustained intervention. This experiment was conducted in two phases. First, in the *priming phase*, we simulated a temporary inhibition of a key target gene (LOXL2, MAPK3, or JUN) by clamping its state to 0 for a specific duration, ranging from 1 to 5 simulation steps. Second, in the *control phase*, the pre-trained PPO agent was given control of the network from its now-primed state. The agent’s success in steering the network to the target sensitive state within the remainder of the 15-step episode was recorded to identify the most effective transient intervention.

2) *Mechanistic Policy Explanation via SHAP*: To gain biological insight into our agent’s decision-making strategy, we employed SHAP (SHapley Additive exPlanations) [22], a game-theoretic explainable AI method that quantifies each feature’s contribution to model predictions by computing average marginal contributions across all possible feature combinations. We applied SHAP to analyze the agent’s policy in two key scenarios: (1) identifying the context-dependent “vulnerability signature” of genes that triggered specific interventions, and (2) assessing how transient priming interventions altered this signature. Additionally, we generated SHAP trajectory visualizations to track the evolution of feature importance over entire control episodes, enabling dynamic interpretation of the agent’s reasoning process.

III. RESULTS AND DISCUSSIONS

A. The Resistant Network is Characterized by a Rigid and Canalized Attractor Landscape

To investigate the dynamic consequences of network rewiring, we performed a computational attractor analysis on both the responder and non-responder PBN models using the *optPBN* MATLAB toolbox [23]. For each PBN, we estimated the attractor landscape by generating an ensemble of 1,000,000 individual Boolean networks (BNs), with each BN stochastically sampled to represent a specific realization of the probabilistic model. We then identified all steady-state and cyclical attractors for each sampled BN. By aggregating these results across all simulations, we calculated the probability of observing each unique attractor, yielding a quantitative map of the system’s dynamics. The results reveal a reorganization of this landscape, shifting from a *plastic*, multi-stable state in responders to a *rigid, canalized* state in non-responders.

The analysis reveals a reorganization of the network’s dynamic landscape, shifting from a plastic, multi-stable state in responders to a rigid, canalized state in non-responders. The responder network exhibits high plasticity, characterized by 22 distinct attractors, with the most probable one accounting for only 12.55% of the total probability basin. In stark contrast, the non-responder network is highly rigid, collapsing into only 16 attractors. A single singleton attractor dominates this landscape, accounting for 50.02% of the total probability, which indicates the network has been rewired to robustly maintain a specific resistant phenotype.

Decoding the dominant attractors provides insight into the specific gene expression patterns that define the sensitive

and resistant states. While the responder landscape was fragmented across multiple phenotypes, the analysis of the non-responder landscape revealed that the dominant attractor did not fully match the expected Innate anti-PD-1 Resistance (IPRES) signature (e.g., $AXL=1$, $WNT5A=1$, $ROR2=1$). The key identified cellular phenotypes are summarized in Table I.

TABLE I: Key cellular phenotypes identified through attractor analysis. Each state is defined by the binary expression (OFF=0, ON=1) of the core IPRES genes AXL , $WNT5A$, and $ROR2$, distinguishing between therapy-sensitive and resistant subtypes.

| Phenotype | Key Gene States (AXL , $WNT5A$, $ROR2$) |
|----------------------------|---|
| Responder (Sensitive) | (0, 0, 1) |
| Resistant (WNT-Driven) | (0, 1, 1) |
| Resistant (AXL -Driven) | (1, 0, 1) |
| Dominant Resistant State | (0, 0, 0) |

This analysis demonstrates that innate resistance corresponds to a fundamental system-level transition to a new, highly stable dynamic regime, where the network becomes *hard-wired* to occupy a dominant, therapy-resistant attractor.

B. Network Rewiring Establishes a $JUN/LOXL2$ Regulatory Axis

Having established that the resistant state is defined by a rigid and dominant attractor, we next sought to identify the specific regulatory changes responsible for this landscape collapse. We performed a comparative analysis of the PBN models, combining a quantitative assessment of gene influence with a detailed inspection of the inferred Boolean logic.

To identify the key regulatory hubs, we calculated a *total influence score* for each gene by summing all its incoming and outgoing edge weights from the network’s influence matrix. This score quantifies a gene’s overall impact as both a regulator and a target within the system. The analysis revealed a significant shift in the network’s command structure, establishing the transcription factor JUN as the unequivocal master regulator of the resistant state, with $LOXL2$ emerging as its primary executive arm. As shown in Figure 1, JUN ’s total influence increases dramatically in the non-responder network, and $LOXL2$ exhibits the second-largest gain. This ascent pinpoints the $JUN/LOXL2$ axis as the central driver of the switch to the therapy-resistant phenotype.

This dramatic rise in influence is the direct result of a fundamental rewiring of both genes’ regulatory logic. In the sensitive responder network, JUN ’s activation is highly conditional, relying on a specific context of present and absent upstream signals. In stark contrast, the logic in the resistant network becomes decisively canalized, collapsing to a simple, robust AND gate that makes JUN ’s activation an “all-or-nothing” event: $JUN = MAP2K3 \text{ AND } NRAS \text{ AND } RELA \text{ AND } LOXL2$. This rewiring creates what is effectively a *hard-wired activation switch* for the master regulator. Concurrently, the regulatory logic for $LOXL2$, the axis’s executive arm,

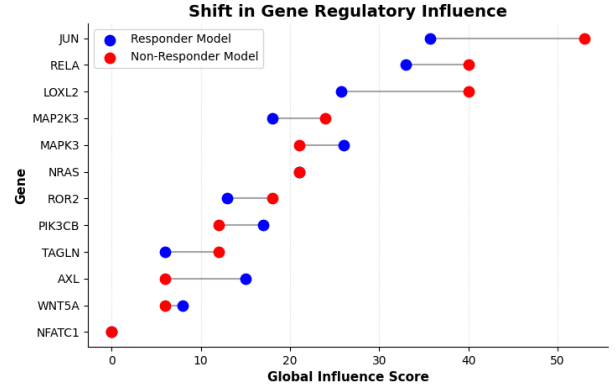


Fig. 1: Shift in total gene influence from the responder (blue) to the non-responder (red) model. The plot highlights the change in influence score for each gene, sorted by their final influence in the non-responder state. The significant increase in JUN ’s influence, along with notable shifts in $LOXL2$, illustrates the systemic rewiring of regulatory control.

undergoes a similar canalization. In the responder network, $LOXL2$ ’s state is determined by a complex, probabilistic mixture of functions. In the resistant network, this complexity collapses into a single, deterministic rule that enslaves $LOXL2$ to its new master regulator: $LOXL2 = JUN \text{ AND } MAP2K3$.

This hierarchical simplification, where JUN is rewired into a master switch and $LOXL2$ is rewired into its direct effector, hard-wires the $JUN/LOXL2$ axis and locks the system into a robustly resistant phenotype.

C. Reinforcement Learning Identifies the $MAP2K3/LOXL2$ Axis as the Optimal Dynamic Control Target

To identify an optimal, unconstrained control policy, we trained a reinforcement learning agent to steer the network from three resistant attractor states to the target sensitive phenotype as in Table I. The resulting policy was exceptionally robust, achieving a 100% success rate over 10,000 evaluation trials.

An analysis of the agent’s actions reveals a highly specific and hierarchical control strategy (Table II). The agent’s policy converged on targeting the $MAP2K3/LOXL2$ axis; its most frequent intervention was to flip $MAP2K3$, followed by flipping $LOXL2$. This demonstrates that while static network analysis pointed to JUN as a master regulator, the dynamic, goal-oriented learning process discovered a more efficient control pathway centered on the upstream kinase $MAP2K3$.

D. Temporal Inhibition Reveals a “Hit-and-Run” Therapeutic Strategy

To identify a clinically relevant, transient intervention strategy, we performed a comprehensive analysis simulating a temporary “priming” inhibition of key targets (JUN , $LOXL2$, and $MAPK3$) for varying durations. After each priming phase, a pre-trained RL agent was tasked with guiding the network to the therapy-sensitive state.

TABLE II: Action frequencies of the trained reinforcement learning agent over 10,000 evaluation episodes. The data reveals a highly specific control policy that converges on flipping MAP2K3/LOXL2 as the primary intervention, identifying it as the optimal dynamic control target.

| Action | Times Chosen |
|--------------------|--------------|
| Flip Gene 'MAP2K3' | 9037 |
| Flip Gene 'LOXL2' | 3366 |
| Flip Gene 'TAGLN' | 659 |
| Flip Gene 'RELA' | 483 |
| Flip Gene 'WNT5A' | 293 |
| Flip Gene 'JUN' | 183 |

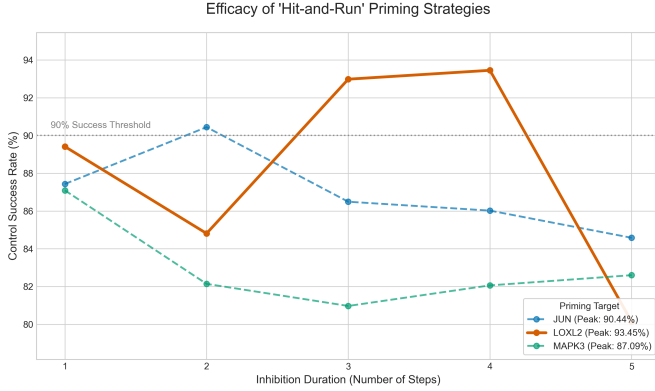


Fig. 2: Efficacy of “hit-and-run” priming strategies. The plot shows the control success rate as a function of the inhibition duration for three key targets. A 4-step inhibition of LOXL2 emerges as the optimal transient strategy, significantly outperforming other interventions.

The results, visualized in Fig. 2, identified a highly effective and specific optimal strategy: a 4-step temporary inhibition of LOXL2, which achieved the highest success rate of 93.45%. The non-monotonic relationship between inhibition duration and success rate for both LOXL2 and JUN provides strong evidence for a “hit-and-run” mechanism, where a precisely timed intervention is more effective than a sustained one. A striking and consistent finding across all experiments was that the agent’s overwhelming post-priming policy was to “Do Nothing”. This validates our hypothesis that a brief, targeted intervention is sufficient to destabilize the resistant network, allowing the system’s own dynamics to complete the transition to a sensitive state.

E. Mechanistic Policy Explanation via SHAP

To deconstruct the sophisticated policy learned by the reinforcement learning agent, we employed SHAP [22]. This allowed us to move beyond observing the agent’s actions to understanding its underlying reasoning, providing mechanistic explanations for its control strategy.

1) *Context-Dependent Intervention Choice:* We sought to understand why the agent prioritizes flipping MAP2K3 over other influential genes like JUN. A comparative SHAP analysis

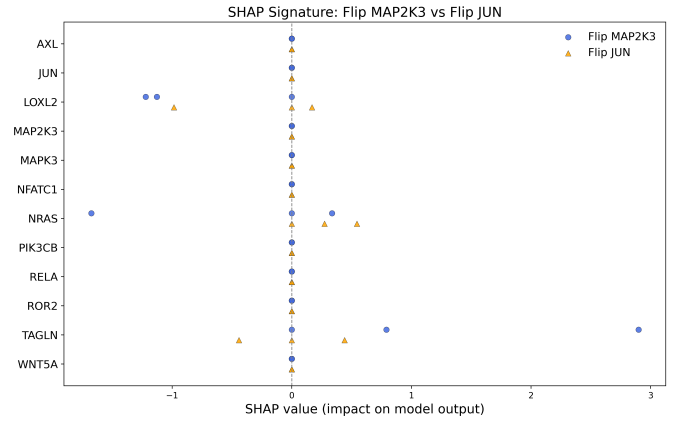


Fig. 3: Comparative SHAP analysis for the agent’s decision to flip MAP2K3 versus JUN from a resistant state. The plot shows the SHAP values for each gene’s contribution to the respective action’s logit, revealing a context-dependent policy.

sis reveals a highly context-dependent policy (Fig. 3). While high LOXL2 states push the agent towards flipping either MAP2K3 or JUN, the states of NRAS and TAGLN act as decisive signals: high NRAS encourages MAP2K3 targeting, while high TAGLN favors JUN intervention.

This context-dependent strategy aligns with melanoma signaling biology. NRAS, mutated in 15-20% of melanomas [24], activates the MAPK cascade through MAP2K3 [25]. The agent’s preference for MAP2K3 in NRAS-high contexts reflects understanding of this upstream-downstream relationship, intercepting oncogenic signals at a strategic chokepoint. Conversely, TAGLN drives cytoskeletal remodeling and epithelial-mesenchymal transition [26], prompting the agent to target JUN—a key AP-1 transcription factor [27]—to disrupt transcriptional programs driving resistance.

This demonstrates that the agent discerns specific molecular contexts rather than identifying a generic resistant state, selecting the most effective pathway-specific intervention and mirroring precision oncology strategies [28].

2) *Validation of the “Hit-and-Run” Mechanism:* Next, we used SHAP to explain why the 4-step inhibition of LOXL2 was more successful than the sub-optimal 2-step inhibition of JUN. We analyzed the network state after each priming strategy by measuring the average SHAP importance of each gene. The results show that the optimal LOXL2 priming is more effective because it does a better job of erasing the “vulnerability signature” that triggers the agent’s desire to intervene (Fig. 4). After the LOXL2 inhibition, the residual SHAP values for key driver genes like NRAS and RELA are significantly lower than after the JUN inhibition, indicating the network has been pushed to a more stable, less-resistant state. The superior efficacy of LOXL2 targeting can be understood through its pleiotropic role in cancer progression. LOXL2 (lysyl oxidase-like 2) functions beyond its canonical role in extracellular matrix crosslinking, acting as a transcriptional regulator that promotes epithelial-mesenchymal transition and stemness [29].

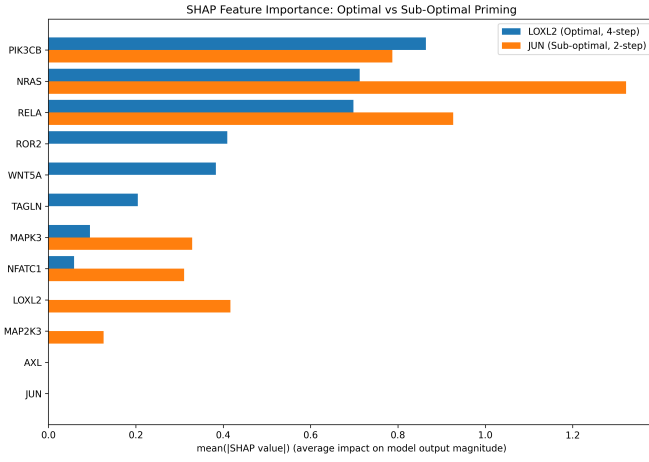


Fig. 4: Comparison of residual SHAP feature importance after the optimal (4-step LOXL2) versus a sub-optimal (2-step JUN) priming strategy. The more effective LOXL2 priming leaves a state with lower overall SHAP importance, requiring less subsequent intervention.

Recent studies have shown that LOXL2 directly interacts with transcription factors including SNAI1 and TWIST1 to drive mesenchymal programs [30], while also stabilizing HIF-1 α under hypoxic conditions [31]. Our finding that LOXL2 inhibition more effectively destabilizes the resistance network aligns with its position as a master coordinator of multiple resistance-associated pathways, including hypoxia response, immune evasion, and metabolic reprogramming [32]. This mechanistic insight supports the growing interest in LOXL2 as a therapeutic target, with several inhibitors currently in clinical development for various cancers [33].

3) *Dynamic Visualization of the Control Strategy*: Finally, to visualize the agent’s reasoning, we analyzed the average of 10,000 simulated 15-step control episodes (Fig. 5). The resulting SHAP trajectory heatmap reveals that the most frequent action at every step was “Do Nothing,” providing strong quantitative support for a “hit-and-run” control mechanism where the network self-corrects after an initial priming.

The heatmap illustrates a persistent “vulnerability signature” that drives the agent’s policy. At the initial step, we observe a powerful negative SHAP contribution from the key driver genes NRAS and RELA, indicating a strong initial impetus for intervention. While this signal weakens after the first step, it does not disappear; instead, it persists at a consistent, lower intensity for the remainder of the episode. This suggests that even as the network evolves, these genes continue to exert a background pressure that the agent has learned to correctly ignore. Other genes, including LOXL2 and MAPK3, contribute weaker, transient negative signals in the early steps before becoming neutral.

This temporal pattern of network self-organization following an initial perturbation aligns with emerging therapeutic paradigms in cancer treatment. The concept parallels successful clinical strategies such as induction chemotherapy in acute

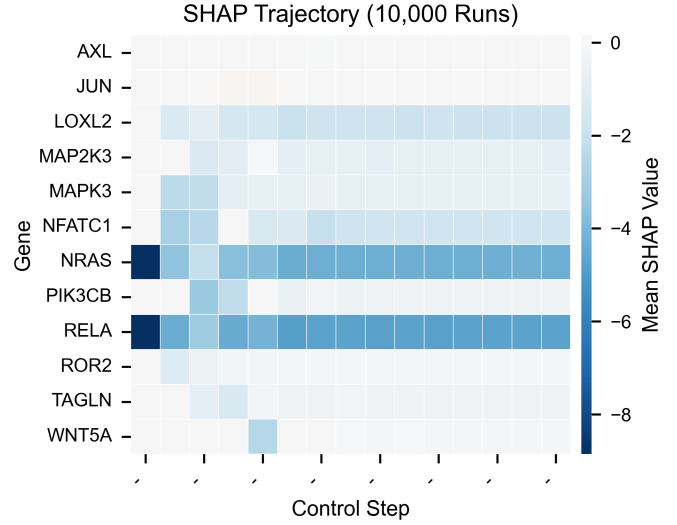


Fig. 5: SHAP trajectory analysis explaining the agent’s policy. The most frequent action was consistently “Do Nothing,” represented by a dash (–) on the x-axis. Persistent negative SHAP values for NRAS and RELA reveal a vulnerability signature that the agent learns to ignore, validating the “hit-and-run” strategy.

leukemias, where intensive initial treatment creates system instability that resolves into remission [34], and immune checkpoint blockade, where brief T-cell activation triggers sustained anti-tumor responses [35]. The identification of NRAS and RELA as key, persistent vulnerability drivers reflects established understanding that RAS/MAPK hyperactivation and NF- κ B inflammatory signaling represent critical resistance mechanisms [1], [36], supporting the biological plausibility of the discovered intervention strategy.

IV. CONCLUSION

This study introduced a novel computational framework integrating PBN modeling, reinforcement learning, and explainable AI to deconstruct and control innate immunotherapy resistance in melanoma. Our analysis revealed that resistance corresponds to a fundamental system-level transition from a plastic, multi-stable network to a rigid, canalized landscape driven by a JUN/LOXL2 regulatory axis that locks the system into a robustly resistant state.

Most significantly, our reinforcement learning approach discovered a non-obvious “hit-and-run” therapeutic strategy: a precisely timed, 4-step temporary inhibition of LOXL2 achieving over 93% success *in silico*. Explainable AI analysis demonstrated that this transient intervention erases the molecular vulnerability signature stabilizing resistance, allowing the network’s intrinsic dynamics to complete the therapeutic transition.

Our findings are based on an *in silico* model with inherent limitations, including its binary gene representation, focus on a core gene set, and the specific reward configuration for reinforcement learning. For instance, using a positive action

cost instead of zero would penalize frequent interventions and could yield a different optimal policy. Consequently, the identified strategies should be interpreted as computational hypotheses that require rigorous experimental validation in cell lines and animal models before any clinical consideration.

The discovery of time-dependent optimal strategies challenges traditional paradigms focused on sustained pathway inhibition. The integrated PBN-RL-XAI pipeline offers a generalizable approach for discovering novel control strategies in complex, treatment-resistant diseases, providing a powerful framework for future therapeutic development.

V. CODE AVAILABILITY

All source code developed for the PBN inference, reinforcement learning, and subsequent analyses presented in this paper are publicly available in our GitHub repository at <https://github.com/Liu-Zhonglin/pbn-melanoma-project>.

ACKNOWLEDGMENT

The author would like to express sincere gratitude to Professor Louxin Zhang for his valuable advice on potential improvements to this work. Special thanks are also extended to Professor Ching Wai Ki for his thorough internal review and constructive feedback.

REFERENCES

- [1] W. Hugo, J. M. Zaretsky, L. Sun, C. Song, B. H. Moreno, S. H. Lieskovan, B. Berent-Maoz, J. Pang, B. Chmielowski, G. Cherry *et al.*, "Genomic and transcriptomic features of response to anti-pd-1 therapy in metastatic melanoma," *Cell*, vol. 165, no. 1, pp. 35–44, 2016.
- [2] P. K. Kreeger and D. A. Lauffenburger, "Cancer systems biology: a network modeling perspective," *Carcinogenesis*, vol. 31, no. 1, pp. 2–8, 2010.
- [3] S. Huang, I. Ernberg, and S. Kauffman, "Cancer attractors: a systems view of tumors from a gene network dynamics and developmental perspective," in *Seminars in cell & developmental biology*, vol. 20, no. 7. Elsevier, 2009, pp. 869–876.
- [4] S. P. Cornelius, W. L. Kath, and A. E. Motter, "Realistic control of network dynamics," *Nature communications*, vol. 4, no. 1, p. 1942, 2013.
- [5] I. Shmulevich, E. R. Dougherty, S. Kim, and W. Zhang, "Probabilistic boolean networks: a rule-based uncertainty model for gene regulatory networks," *Bioinformatics*, vol. 18, no. 2, pp. 261–274, 2002.
- [6] S.-Q. Zhang, W.-K. Ching, M. K. Ng, and T. Akutsu, "Simulation study in probabilistic boolean network models for genetic regulatory networks," *International Journal of Data Mining and Bioinformatics*, vol. 1, no. 3, pp. 217–240, 2007.
- [7] R. S. Sutton, A. G. Barto *et al.*, *Reinforcement learning: An introduction*, vol. 1, no. 1.
- [8] A. Mardt, L. Pasquali, H. Wu, and F. Noé, "Vampnets for deep learning of molecular kinetics," *Nature communications*, vol. 9, no. 1, p. 5, 2018.
- [9] B. Durbin, J. Hardin, D. Hawkins, and D. Rocke, "A variance-stabilizing transformation for gene-expression microarray data," *Bioinformatics*, vol. 18, 2002.
- [10] M. I. Love, W. Huber, and S. Anders, "Moderated estimation of fold change and dispersion for rna-seq data with deseq2," *Genome biology*, vol. 15, no. 12, p. 550, 2014.
- [11] D. Reynolds, "Gaussian mixture models," in *Encyclopedia of biometrics*. Springer, 2015, pp. 827–832.
- [12] I. Shmulevich, E. R. Dougherty, and W. Zhang, "From boolean to probabilistic boolean networks as models of genetic regulatory networks," *Proceedings of the IEEE*, vol. 90, no. 11, pp. 1778–1792, 2002.
- [13] W. Haynes, "Benjamini-hochberg method," in *Encyclopedia of systems biology*. Springer, 2013, pp. 78–78.
- [14] S. Anders and W. Huber, "Differential expression analysis for sequence count data," *Nature Precedings*, pp. 1–1, 2010.
- [15] V. A. Huynh-Thu and P. Geurts, "dyngen3: dynamical genie3 for the inference of gene networks from time series expression data," *Scientific reports*, vol. 8, no. 1, p. 3384, 2018.
- [16] A. Kraskov, H. Stögbauer, and P. Grassberger, "Estimating mutual information," *Physical Review E—Statistical, Nonlinear, and Soft Matter Physics*, vol. 69, no. 6, p. 066138, 2004.
- [17] Z. Ma, Z. J. Wang, and M. J. McKeown, "Probabilistic boolean network analysis of brain connectivity in parkinson's disease," *IEEE Journal of selected topics in signal processing*, vol. 2, no. 6, pp. 975–985, 2009.
- [18] A. Mizera and J. Zarzycki, "pbn-stac: Deep reinforcement learning-based framework for cellular reprogramming," *Theoretical Computer Science*, p. 115382, 2025.
- [19] M. L. Puterman, "Markov decision processes," *Handbooks in operations research and management science*, vol. 2, pp. 331–434, 1990.
- [20] J. Schulman, F. Wolski, P. Dhariwal, A. Radford, and O. Klimov, "Proximal policy optimization algorithms," *arXiv preprint arXiv:1707.06347*, 2017.
- [21] A. Raffin, A. Hill, A. Gleave, A. Kanervisto, M. Ernestus, and N. Dormann, "Stable-baselines3: Reliable reinforcement learning implementations," *Journal of machine learning research*, vol. 22, no. 268, pp. 1–8, 2021.
- [22] S. M. Lundberg and S.-I. Lee, "A unified approach to interpreting model predictions," *Advances in neural information processing systems*, vol. 30, 2017.
- [23] P. Trairatphisan, A. Mizera, J. Pang, A. A. Tantar, and T. Sauter, "optpbn: An optimisation toolbox for probabilistic boolean networks," *PloS one*, vol. 9, no. 7, p. e98001, 2014.
- [24] P. A. Ascierto, J. M. Kirkwood, J.-J. Grob, E. Simeone, A. M. Grimaldi, M. Maio, G. Palmieri, A. Testori, F. M. Marincola, and N. Mozzillo, "The role of braf v600 mutation in melanoma," *Journal of translational medicine*, vol. 10, pp. 1–9, 2012.
- [25] B. B. Domingues, "Possible therapies to overcome resistance to mapk inhibitors in mutant braf melanoma," Master's thesis, Universidade do Porto (Portugal), 2018.
- [26] K.-H. Tsui, Y.-H. Lin, K.-S. Chang, C.-P. Hou, P.-J. Chen, T.-H. Feng, and H.-H. Juang, "Transgelin, a p53 and pten-upregulated gene, inhibits the cell proliferation and invasion of human bladder carcinoma cells in vitro and in vivo," *International journal of molecular sciences*, vol. 20, no. 19, p. 4946, 2019.
- [27] J. Hess, P. Angel, and M. Schorpp-Kistner, "Ap-1 subunits: quarrel and harmony among siblings," *Journal of cell science*, vol. 117, no. 25, pp. 5965–5973, 2004.
- [28] A. M. Tsimberidou, E. Fountzilas, M. Nikanjam, and R. Kurzrock, "Review of precision cancer medicine: Evolution of the treatment paradigm," *Cancer treatment reviews*, vol. 86, p. 102019, 2020.
- [29] H. E. Barker, T. R. Cox, and J. T. Erler, "The rationale for targeting the lox family in cancer," *Nature Reviews Cancer*, vol. 12, no. 8, pp. 540–552, 2012.
- [30] D. H. Peng, C. Ungewiss, P. Tong, L. A. Byers, J. Wang, J. R. Canales, P. A. Villalobos, N. Uraoka, B. Mino, C. Behrens *et al.*, "Zeb1 induces lox12-mediated collagen stabilization and deposition in the extracellular matrix to drive lung cancer invasion and metastasis," *Oncogene*, vol. 36, no. 14, pp. 1925–1938, 2017.
- [31] R. Schietke, C. Warnecke, I. Wacker, J. Schödel, D. R. Mole, V. Campean, K. Amann, M. Goppelt-Strube, J. Behrens, K.-U. Eckardt *et al.*, "The lysyl oxidases lox and lox12 are necessary and sufficient to repress e-cadherin in hypoxia: insights into cellular transformation processes mediated by hif-1," *Journal of Biological Chemistry*, vol. 285, no. 9, pp. 6658–6669, 2010.
- [32] L. E. Tracy, R. A. Minasian, and E. Caterson, "Extracellular matrix and dermal fibroblast function in the healing wound," *Advances in wound care*, vol. 5, no. 3, pp. 119–136, 2016.
- [33] T. Peng, S. Lin, Y. Meng, P. Gao, P. Wu, W. Zhi, W. Ding, C. Cao, and P. Wu, "Lox12 small molecule inhibitor restrains malignant transformation of cervical cancer cells by repressing lox12-induced epithelial-mesenchymal transition (emt)," *Cell Cycle*, vol. 21, no. 17, pp. 1827–1841, 2022.
- [34] M. S. Tallman, E. S. Wang, J. K. Altman, F. R. Appelbaum, V. R. Bhatt, D. Bixby, S. E. Coutre, M. De Lima, A. T. Fathi, M. Fiorella *et al.*, "Acute myeloid leukemia, version 3.2019, nccn clinical practice guidelines in oncology," *Journal of the National Comprehensive Cancer Network*, vol. 17, no. 6, pp. 721–749, 2019.

- [35] A. Ribas, W. N. Haining, and T. N. Schumacher, "When cancer cells become the enablers of an antitumor immune response," *Cancer Discovery*, vol. 12, no. 10, pp. 2244–2248, 2022.
- [36] M. E. Bahar, H. J. Kim, and D. R. Kim, "Targeting the ras/raf/mapk pathway for cancer therapy: from mechanism to clinical studies," *Signal transduction and targeted therapy*, vol. 8, no. 1, p. 455, 2023.